Design of a 100 W, 500000 rpm Permanent-Magnet Generator for Mesoscale Gas Turbines

C. Zwyssig and J.W. Kolar
Power Electronic Systems Laboratory
Swiss Federal Institute of Technology Zurich
8092 Zurich, SWITZERLAND
zwyssig@lem.ee.ethz.ch

W. Thaler and M. Vohrer

ATE Antriebstechnik und Entwicklungs GmbH
88299 Leutkirch, GERMANY
w.thaler@ate-system.de

***Abstract*—Mesoscale gas turbine generator systems are a promising solution for high energy and power density portable devices. This paper focuses on the design of a 100 W, 500000 rpm generator suitable for use with a gas turbine. The design procedure selects the suitable machine type and bearing technology, and determines the electromagnetic characteristics. The losses caused by the high frequency operation are minimized by optimizing the winding and the stator core material. The final design is a permanent-magnet machine with a volume of 3.5 cm^3 and experimental measurements from a test bench are presented.**

Keywords - Generator design; permanent-magnet; high-speed; gas turbines; portable power

I. INTRODUCTION

The increasing need for high energy density portable power devices has led to intense research and development efforts on mesoscale systems with power outputs up to a hundred Watts [1]. In this power range traditional batteries are challenged by devices that use fuel since the fuel provides significantly higher chemical energy density.

An especially promising way of converting the energy stored in the fuel into electrical energy is to use gas turbine generator sets. Accordingly, several international research groups are downscaling traditional gas turbines. For example, researchers at the Tohoku University, Japan, are building a 100 W, 870000 rpm gas turbine [2] and a team at the Stanford University, USA, has demonstrated a compressor/turbine assembly running at 420000 rpm with a design speed of 800000 rpm [3]. A turbine designed at K.U. Leuven, Belgium, has an electrical power output of 44 W at a speed of 160000 rpm when coupled to a low power commercial generator [4].

All power supply systems of this type require an electrical system consisting of a high-speed generator/starter, power electronics, a control platform and a form of energy storage to power the starting of the turbine (Fig. 1). However, the research so far has only concentrated on the turbine design, and very little research effort has occurred on determining the requirements and the design of the electrical system. Therefore, this paper focuses on the design of a high-speed generator with a rated speed of 500000 rpm and an electrical power output of 100 W. The main challenges of the generator design are the losses due to the high frequency in the stator core and windings, the bearing technology, the rotor dynamics and the thermal design with rotor temperatures up to 300 °C resulting from the close proximity to the gas turbine.

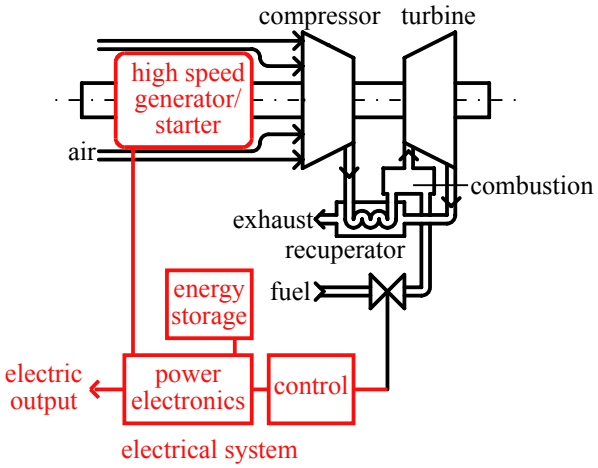

Figure 1. components of a gas turbine generator set.

The design method starts with the selection of the machine type and the bearing technology, then the magnetic and electric characteristics are obtained with the help of finite-element methods. Losses in the windings and in the stator core are determined by analytical calculations. To verify the dimensioning, a test bench setup is realized including mechanical stress analysis and rotor dynamics. Finally, first measurements for reduced speed operation are presented.

II. MACHINE SELECTION

There are two basic concepts of electromechanical energy conversions, machines based either on electric or magnetic fields. At the required power level and for the expected machine dimensions in the millimeter range, a magnetic machine is the better choice [7].

The rated current of a magnetic machine scales proportional with the machine dimensions [8]. Therefore, the flux density in an electrically excited motor, e.g. induction machines (IM) or switched reluctance machines (SRM), decreases with decreasing size. In contrary, permanent magnet flux density remains constant for decreasing machine volume. Therefore,

only permanent magnet machines are considered with the aim for a low system volume.

High-speed operation requires a simple and robust rotor geometry and construction. A commutation system employed for the current commutation in dc machines produces additional friction and limits the speed (to typically 25000 rpm). Therefore, the only machine types left that meet both small size and high-speed requirements are the brushless dc (BLDC) machine, fed by square-wave currents, and the identically constructed permanent magnet synchronous machine (PMSM), fed by sinusoidal currents. For these machines both slotless and slotted stators could be employed. In [9] the slotless configuration is found to be the better choice for high-speed operation because of the simpler manufacturing of the stator core and the reduction of eddy current losses in the rotor (no slotting harmonics and less armature current reaction).

The generator volume can be estimated with scaling laws that have been verified by investigating existing small permanent-magnet motors [8]. There, a torque-per-volume constant of C = 0.0006 Nm/cm^3 is identified. It is found that the friction (mechanical friction and magnetic stator core losses) is approximately 5% of the generated torque, although there is a wide variation for the analyzed motors. With a friction of 10% of the produced torque the generator volume V is estimated as

$$V = 1.1\frac{60P_r}{2\pi n_r}\frac{1}{C} = 3.5\ cm^3 . \qquad (1)$$

III. Bearing Selection

For machine speeds in the range of 500000 rpm the selection of a suitable bearing is a main issue. In this section the possible choices are compiled and briefly compared.

High-speed ball bearings are commonly used in the dental industry, and bearings are available for speeds exceeding 500000 rpm. The main advantages of ball bearings are the robustness and small size. The main disadvantages are the limited operating temperature and a lifetime dependent on lubrication, load and speed.

Static air bearing, dynamic air bearings and foil bearings levitate the rotor with air pressure, either generated with an external supply (static) or by spinning the rotor (dynamic and foil). They all show low friction losses and a long lifetime. Foil bearings are reported for speeds up to 700000 rpm and temperatures up to 650 °C [11], but are not commercially available and require a complex design procedure.

Magnetic bearings levitate the rotor using magnetic forces and have similar advantages as air bearings. However, active magnetic bearings require sensors, actuators and control, which results in high complexity and increased bearing volume.

In summary, all bearings apart form ball bearings have no wear and just air friction and therefore a long lifetime and low losses. However, due to the simplicity, robustness, small size and avoidance of auxiliary equipment, ball bearings are selected for a first test bench setup. Foil bearings are an interesting alternative, especially for higher operating temperatures, and are considered further.

IV. Electromagnetic Design

The electromagnetic machine design is carried out with the help of the finite-element software FEMAG [12] for a rated power of 100 W at a speed of 500000 rpm in a compact and simple design.

The volume is set to the value calculated with (1) and a length-to-diameter ratio of 1:1 is defined. This leads to a short shaft which increases the critical speed. The machine has an active length of 15 mm and a stator diameter of 16 mm.

The peak value of the back EMF is set to 16 V in order to allow the use of low on-resistance power MOSFETs in the power electronic converter.

A. Rotor

The dimensions for the rotor are mainly defined by mechanical aspects such as inner bearing diameter (3.175 mm), rotor dynamics, centrifugal forces, prevention of unbalance and manufacturability.

The permanent magnet can be realized as one cylindrical piece. Beside simple manufacturing this has the advantage of producing a sinusoidal air gap field. For highest torque density, high-energy rare earth magnets such as sintered NdFeB or SmCo are the only choices. An Sm_2Co_{17} based magnet is chosen because of its outstanding thermal characteristics (operating temperatures up to 350 °C).

A retaining sleeve is used in order to limit the centrifugal force stress on the brittle magnet. The outer rotor diameter is 6 mm.

B. Stator

The stator consists of the stator core and the winding. Both are optimized with respect to losses (Section IV.D.2 and IV.D.3). Two possibilities for the slotless winding structure, a ring-wound, i.e a toroidal winding around the stator core (Fig. 2) and a cup-shaped surface winding on the inner side of the stator core are considered.

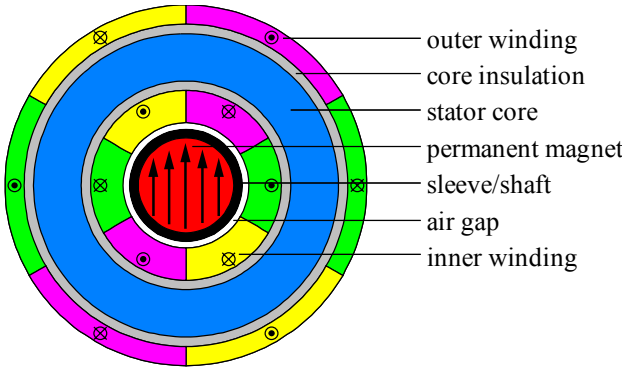

Figure 2. Layout of the slotless brushless permanent-magnet generator with ring-wound stator. The rotor diameter is 6 mm, the stator core inner diameter is 11 mm, the stator core outer diameter is 16 mm and the active length is 15 mm.

C. Finite Element Calculations

The results of finite-element simulations presented in this section are carried out for the generator layout according to Fig. 2. The sinusoidal magnetic flux density has a peak value of 0.32 T in the middle of the air gap. The voltage is sinusoidal and the desired peak value of 16 V is achieved with two nine-turn windings connected in series (Fig. 3). For a power output of 100 W at a speed of 500000 rpm the torque has to be 1.9 mNm, and this is produced by either a sinusoidal current of 4.1 A peak (2.9 A rms) or a squarewave current with an amplitude of 3.7 A (Fig. 4). Depending on the armature current waveform, the produced electrical torque is either constant or contains a ripple component (Fig. 5).

D. Losses

In addition to electric losses in rotor and stator, there are friction losses in the bearings and air friction losses of the rotor. The standard loss calculation for ball bearings is not valid anymore for these high speeds and air friction is difficult to calculate. Therefore both these losses are determined experimentally using a test bench.

1) Electric Rotor Losses

Electric rotors losses occur in the sleeve and permanent magnet due to eddy currents induced by variations in the flux density with respect to the rotor. In slotless machines this is only due to the switching frequency armature current ripple and the phase cyclic commutation in the case of square-wave currents. For sinusoidal currents, the field due to the armature currents rotates synchronously with the rotor and this does not cause flux density variations and therefore no losses.

Due to the large air gap of a slotless BLDC machine the flux density on the surface of the rotor caused by square-wave armature currents is about a factor 1000 lower than the flux density generated by the permanent magnet. Therefore, the losses are negligible compared to the bearings and air friction losses.

2) Stator Winding Losses

The fundamental frequency in the stator at rated speed is $f_s = 8.3$ kHz. At this frequency, the skin effect has to be taken into account. Furthermore, the active part of the winding is exposed to the magnetic field produced by the permanent magnet that rotates with the same frequency. This results in additional eddy current losses. These two losses can be calculated separately and then summed up [13]. The proximity effect is not considered, because the field caused by the permanent magnet is much larger than the field resulting from neighboring wires.

For a single round wire the losses caused by the dc resistance and the skin effect are given by (2). The losses caused by the external magnetic field are independent of the current as can be seen from (3). The total losses $P_{tot} = P_s + P_p$ have a minimum for a certain diameter because (2) decreases and (3) increases with increasing diameter (Fig. 6).

$$P_s = \frac{\hat{I}^2}{2} F \qquad (2)$$

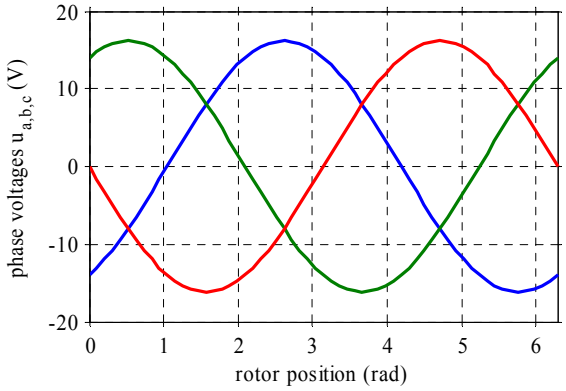

Figure 3. Back EMF of the three phases obtained by finite-element simulations.

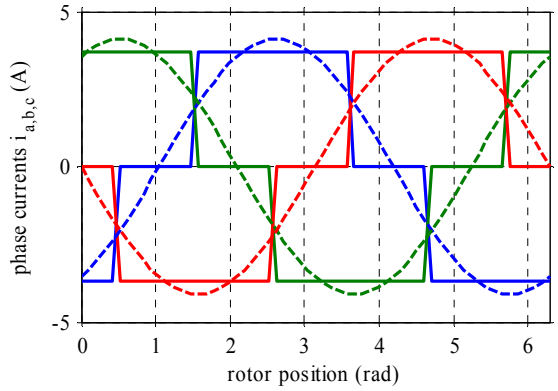

Figure 4. Impressed armature currents of the three phases, either sinusoidal or squarewave.

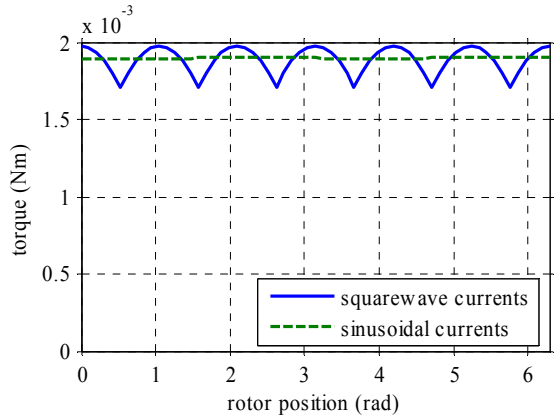

Figure 5. Resulting torque obtained by finite-element simulations. The torque ripple due to square-wave currents is clearly visible.

$$P_p = H_e^2 G \qquad (3)$$

where $\hat{I}$ is the peak current and H_e the peak magnetic field strength, and the coefficients F and G are dependent on the conductor diameter, length, conductivity and frequency.

By using litz wire the current in each turn is divided into strands. For any number of strands, and a resulting current per

strand, there exists an optimal strand diameter. With this optimal diameter, the total copper losses of the generator can be calculated for different number of strands (Fig. 7). Above one hundred strands the losses decrease only slightly. A diameter of 0.071 mm is commonly available and then the ideal number of strands is 60. This results in total copper losses of $P_{V,Cu} = 1.85$ W and the used area including isolation is $A_w = 7.5$ mm^2, which is still below the available winding area of $A_{w,a} = 8.3$ mm^2.

3) Stator Core Losses

In the stator core, the magnetic field rotates with high frequency (8.3 kHz) and therefore, a high frequency stator core material is required. Possible choices are:

1. Silicon-iron, 168 µm laminations
2. Amorphous iron-based materials
3. Nanocrystalline iron-based materials
4. Ferrite
5. Nickel-iron, 100 µm laminations
6. Soft magnetic composites

For sinusoidal induction the core losses for most magnetic materials can be determined using the Steinmetz equation

$$P_{V,core} = C_m \cdot f^{\alpha} \cdot B_m^{\beta} \qquad (4)$$

where C_m, α and β are directly taken from datasheets or calculated from core loss curves using a least square method. For a first comparison of the materials, the stator core losses are calculated for a frequency of f = 10 kHz and a peak magnetic flux density of $B_m = 0.5$ T (Table I).

Due to the lowest losses and the high Curie temperature nanocrystalline materials look very promising. However, currently only ring tape cores are manufactured. This is optimal for power inductors and transformers, where the magnetic flux flows along the core. But in the generator the magnetic flux lines enter the core in radial direction, which results in higher eddy current losses in the vicinity of the entering areas.

In high-speed motors for the dental industry, mainly Ni-Fe is used as stator core material. As an example, in a Ni-Fe core with a volume of 1.6 cm^3, a peak flux density of 0.5 T and a frequency of 10 kHz, stator core losses of $P_{V,core} = 1.2$ W occur.

V. Thermal Analysis

The thermal analysis of the generator depends strongly on the design and the mechanical coupling to the gas turbine. Due to the small size of the whole system and the close proximity of the generator to the turbine, high generator operating temperatures are to be expected. Therefore, the temperature limits for different materials are determined and compared, in order to insure the highest possible operating temperature. From Table II it can be seen that the stator core material is limiting the temperature to values below 200 °C, if Si-Fe is not considered. A meaningful thermal analysis can only be undertaken for an integrated system with a gas turbine.

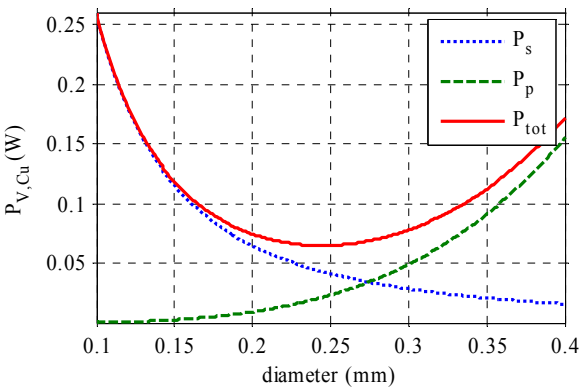

Figure 6. Losses of one copper conductor (P_{tot}) versus diameter of the conductor. The conductor has a length of 15 mm, an amplitude of the sinusoidal current of $\hat{I} = 4$ A with a frequency of 8.3 kHz, in a sinusoidal magnetic field of $H_e = 255$ kA/m ($B = 0.32$ T) with the same frequency.

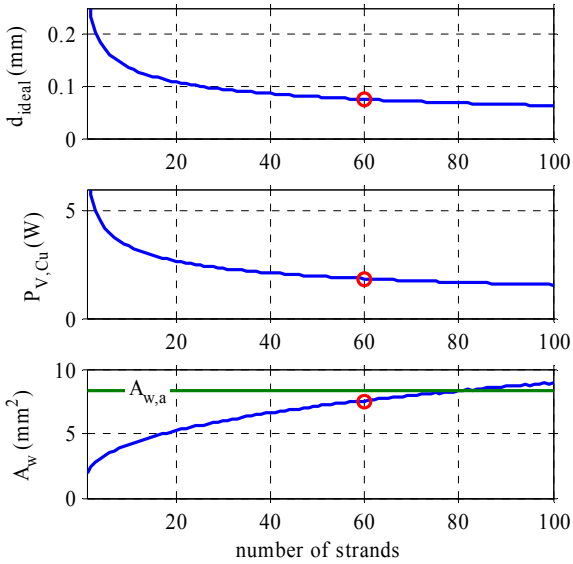

Figure 7. Ideal diameter of one strand (d_{ideal}), total generator copper losses ($P_{V,Cu}$) and resulting winding area (A_w) versus number of strands. A_w is calculated with a copper filling factor of 0.31. The available winding area is $A_{w,a} = 8.3$ mm^2. The average magnetic flux in the winding is $B = 0.32$ T at a frequency of 8.3 kHz.

TABLE I. Core Material Properties

	Density (g/cm^3)	Curie temp. (°C)	Rel. perm. μ_r	Sat. B_{max} (T)	Losses[a] (W/cm^3)
1. Si-Fe	7.6	740	2000	1.7	3.5
2. Am.	7.29	358	<20000	1.41	0.15
3. Nanoc.	7.3	570	<70000	1.3	0.02
4. Ferrite	4.85	120	<15000	0.5	0.175
5. Ni-Fe	8.2	310	<80000	1.48	0.746
6. SMC	3.18	450	<500	2	2.8

a. Losses at a frequency of 10 kHz and a peak flux density of 0.5 T.

TABLE II. MAXIMUM OPERATING TEMPERATURES

Permanent magnet	**Max. operating temp.**
Sm_2Co_{17}	350 °C
High-speed ball bearings	
High-speed lubrication	200 °C
Copper litz wire	
Typical insulation	Class F, 155 °C
High temperature insulation	240 °C
Stator core	
Amorphous/nanocrystalline	150 °C
Ni-Fe	180 °C

VI. MECHANICAL ANALYSIS

The centripetal body load of a rotor with density ρ increases proportional with the radius r and with the square of the angular velocity ω

$$F = \rho \cdot r \cdot \omega^2 . \quad (5)$$

Therefore, two main issues have to be considered: First, the stresses in the cylindrical permanent magnet and the sleeve and second, the contact pressure in between the magnet and the sleeve. Both can be calculated analytically [14] and with 2D finite element simulations.

A. Mechanical Stresses

The permanent magnet material used in the rotor ideally has a high compressive strength (800 MPa) and a medium flexural strength (120 MPa) (Table III), but it is very brittle. Therefore, the stresses on the magnet due to high speeds are limited by a steel or titanium retaining sleeve with an interference fit assembly achieved by shrinkage.

The biggest stresses in the whole rotor occur on the inner side of the retaining sleeve. For a titanium alloy sleeve and interference fit of 15 µm the tangential stress σ_θ becomes 300 N/mm^2 at standstill and 325 N/mm^2 at rated speed (Fig. 8, Fig. 9). The main part of the stress is due to the interference fit, whereas the body load due to rotation only adds 25 N/mm^2 at the critical inner side of the retaining sleeve.

To ensure a safe area of operation the Von Mises stress σ_V [14] is calculated from (6) and compared to the tensile stress of the materials for standstill up to rated speed.

$$\sigma_V = \sqrt{\sigma_r^2 + \sigma_\theta^2 - \sigma_r \sigma_\theta} \quad (6)$$

where σ_θ denotes the tangential stress and σ_r the radial stress component. This leads to a maximum Von Mises stress at the inner side of the titanium sleeve of 328 N/mm^2 for standstill and 347 N/mm^2 for rated speed respectively, which is a sufficient safety margin to the tensile strength of titanium (Table III). The stresses in the permanent magnet are low for standstill up to rated speed. The 2D finite element simulations correspond to the calculations within less than 1%. Fig. 10 and 11 show the Von Mises stresses for a quarter of the rotor. The rotor setup is analysed for room temperature (23 °C). At higher temperatures the stresses decrease due to the larger coefficient of thermal expansion (CTE) of the sleeve material compared to the permanent magnet material.

TABLE III. MECHANICAL PROPERTIES OF ROTOR MATERIALS

	Titanium grade 5	**Austenitic steel**	**Permanent magnets**
Alloy	Ti-6Al-4V	Fe, Cr, Mn, Mo, N	Sm_2Co_{17}
Density	4.4 g/cm^3	8 g/cm^3	8.3 g/cm^3
Modulus of Elasticity	114 GPa	180 GPa	190 GPa
Tensile Strength	895 MPa	975 MPa	120[a]/800[b] MPa
Yield strength	826 MPa	615 MPa	120[a]/800[b] MPa
Coefficient of thermal exp.	9.1e-6 1/K	15.5e-6 1/K	8-11e-6 1/K

a. flexural strength, b. compressive strength.

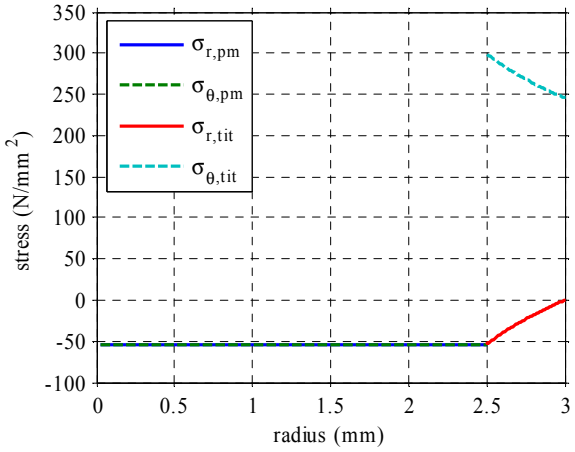

Figure 8. Stresses in Sm_2Co_{17} permanent magnet and titanium sleeve at standstill and a temperature of 23 °C and an interference fit of 15 µm.

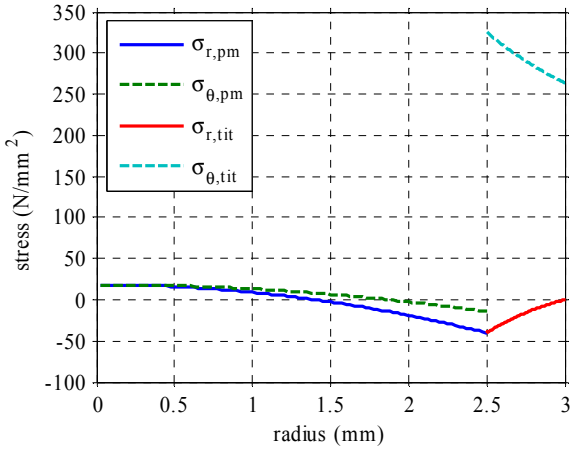

Figure 9. Stresses in Sm_2Co_{17} permanent magnet and titanium sleeve for a speed of 500000 rpm and a temperature of 23 °C and an interference fit of 15 µm.

B. Contact Pressure

With increasing speed the interference fit loosens due to the body load. The contact pressure must be large enough over the whole speed range in order to guarantee the torque transfer

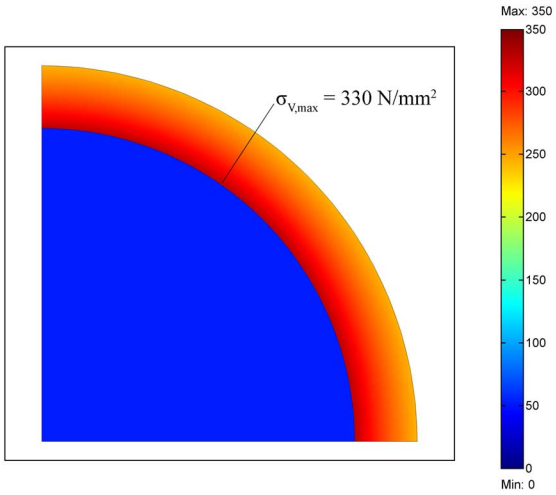

Figure 10. Von Mises Stresses (N/mm^2) in Sm_2Co_{17} permanent magnet and titanium sleeve at standstill and a temperature of 23 °C and an interference fit of 15 µm.

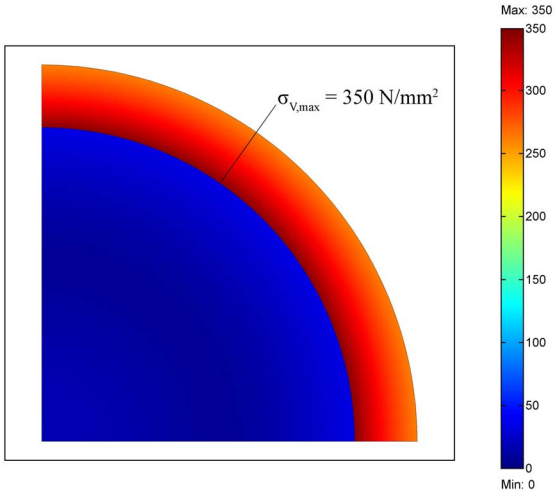

Figure 11. Von Mises Stresses (N/mm^2) in Sm_2Co_{17} permanent magnet and titanium sleeve for a speed of 500000 rpm and a temperature of 23 °C and an interference fit of 15 µm.

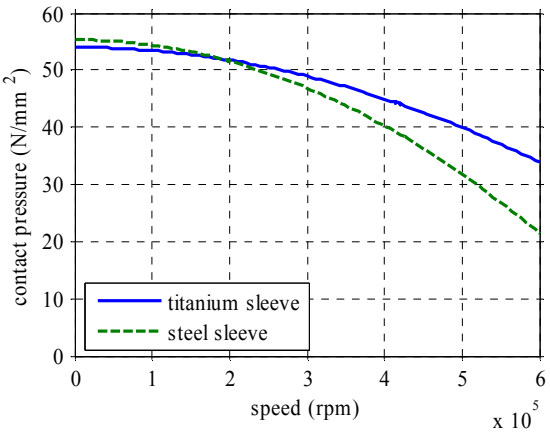

Figure 12. Contact pressure between the permanent magnets and the sleeve as a function of the speed at a temperature of 23 °C and an interference fit of 15 µm for titanium and 10 µm for steel.

from the permanent magnet to the retaining sleeve, which also acts as shaft (Fig. 13). With a titanium sleeve the contact pressure decreases less with increasing speed because the modulus of elasticity compared to the density is higher than for steel (Fig. 12). The contact pressure is calculated for room temperature (23 °C). At higher temperatures the interference fit loosens due to the larger CTE of the sleeve material compared to the permanent magnet material. Therefore titanium is the preferred sleeve material as it has a similar CTE as the permanent magnet material. This means that the contact pressure stays relatively constant as a function of temperature compared to steel.

VII. Test Bench

An experimental test bench is built in order to verify theoretical considerations and the generator concept. As no turbine with the appropriate specifications is presently available, two machines are arranged on a common shaft, one is operated as driving motor, and one as generator. The rotor is supported by two radial single row high-speed ball bearings and contains two permanent magnets, one for each machine. The stator is wound according to Fig. 2. Fig. 13 shows a cut away representation of the test bench setup.

A. Rotor Dynamics

In order to run the test bench in between two critical speeds, the bending modes of the rotor are determined with finite element simulations. The spring constant of the bearing system is taken into account, which shifts the bending modes to lower frequencies. The length of the shaft is adjusted such that rated speed (500000 rpm, 8333 Hz) falls between the second and the third bending modes. This is verified by the results given in Fig. 14 and Table IV.

B. Hardware

Different winding types and core materials are to be tested to determine the various electric and magnetic losses. For the first test bench configuration the rotor consists of a titanium retaining sleeve integrating two diametrically magnetized Sm_2Co_{17} permanent magnets (one for the motor and one for the generator). The stator is a ring-wound litz wire around a Ni-Fe core. One phase consists of two nine-turn windings connected in series and the three phases are star-connected. The core has a volume of 1.6 cm^3 and the overall machine volume is 5 cm^3. The active length of one machine is 15 mm. The individual parts can be seen in Fig. 15.

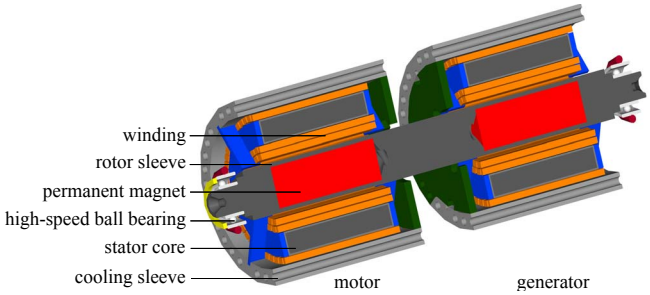

Figure 13. Test bench setup with two machines on a common shaft.

TABLE IV. BENDING MODES

Sleeve material	Titanium	Steel
First bending mode	2400 Hz	2300 Hz
Second bending mode	4250 Hz	3730 Hz
Third bending mode	9880 Hz	9020 Hz

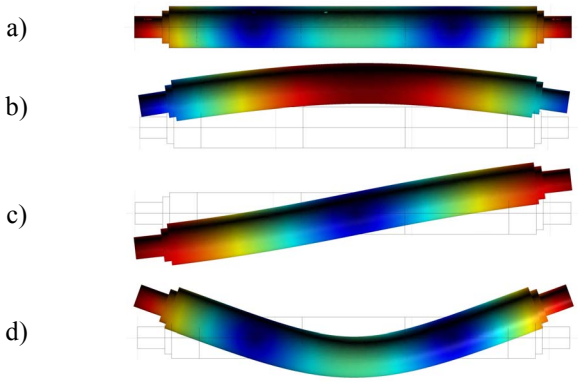

Figure 14. Bending modes of the rotor in the test bench. Standstill (a), first bending mode (b), second bending mode (c) and third bending mode (d).

C. *Torque Sensor*

The torque is transformed with a moment arm into a force. With a distance of 50 mm the rated torque of 1.9 mNm is translated into a force of 38 mN or a weight of 3.9 g. To measure this small force a special piezoresistive sensor is employed in the test bench. The sensor has a measurement range of 0 to 530 mN and a linearity of <0.2% full scale (FS). This results in an accuracy for the torque of better than 0.053 mNm. The sensor is ideal for static measurements because of its long term stability of less than 0.5% FS. Fig. 16 shows the whole test bench including the torque measurement setup.

VIII. MEASUREMENTS

With all the parts assembled in the test bench, the theoretical results are verified with initial measurements. The motor is driven open loop with an impressed three phase current of 2.5 A that is of adjustable frequency. For the first tests an impressed current with a frequency of 833 Hz is used to rotate the motor and generator at 50000 rpm. The speed is limited because of the current source driving the motor and further refinements required to hold the stator winding in place.

From the no-load test on the generator side a back EMF of 1.6 V peak at 50000 rpm is measured. Since the back EMF is proportional to the speed this matches the 16 V peak for 500000 rpm predicted by finite element analysis. As can be seen from Fig. 17 the back EMF is perfectly sinusoidal.

An adjustable resistive three phase load is then connected to the generator side. The generator phase currents are varied between 0.6 A and 2 A, the torque is measured and compared to the finite-element calculations. Again, there is a very good agreement between predictions and tests (Fig. 18). At these low torques the measurement has to be carried out very carefully.

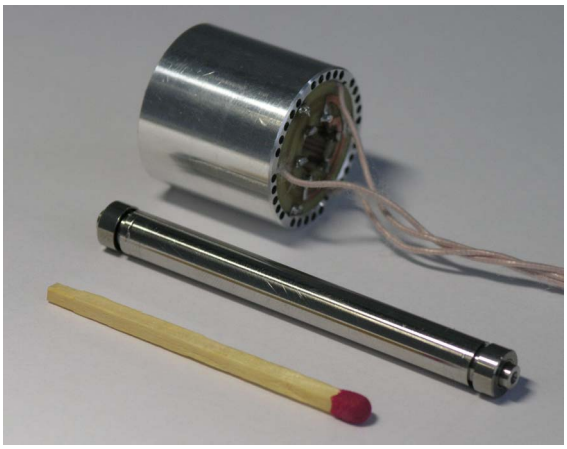

Figure 15. One stator and the common rotor with mounted ball bearings of the test bench.

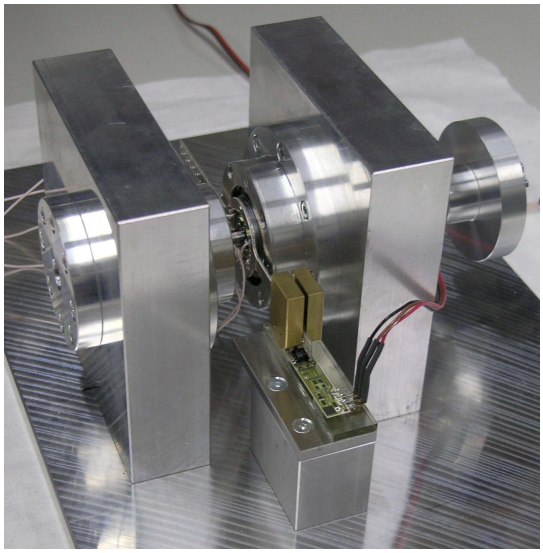

Figure 16. Test bench with motor in the left and generator in the rigth flange. The piezoresistive force sensor in the fornt of the picture is preloaded to half of its full scale.

Small forces from vibrations and the wiring can influence the results.

IX. FUTURE STEPS

In order to spin the rotor at the desired 500000 rpm suitable power electronics and sensorless control for both motor and generator will be built. The challenges are the high switching frequency due to the already high fundamental frequency of 8.3 kHz and the voltage measurement due to the low back EMF at low speed. Efficiency and loss measurements will be carried out for different stator materials, including amorphous and nanocrystalline alloys which should show lower losses than standard machine core materials. A cup-shaped surface winding will also be tested instead of the ring-wound type. However, this is a trade off between volume and losses. The desired result of these measurements is to produce an optimal high-speed low power generator.

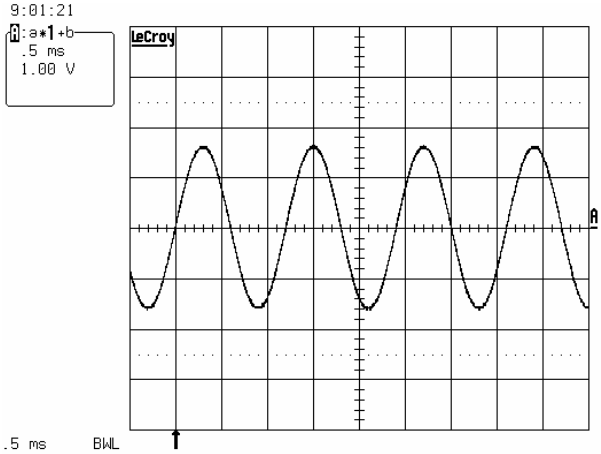

Figure 17. Measured back EMF of the generator in the test bench at 50000 rpm (0.5 ms/div, 1 V/div).

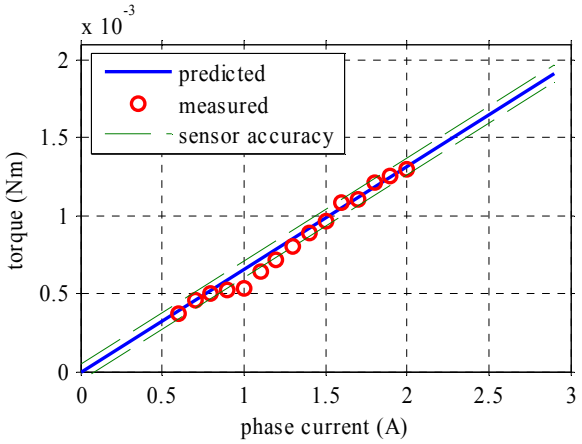

Figure 18. Comparison of predicted and measured torque over phase current.

X. Conclusion

A high-speed, 100 W, 500000 rpm permanent magnet generator design for mesoscale gas turbines has been presented in this paper. The integral design method includes the machine type and bearing selection, the electromagnetic and the mechanical design. The losses in the copper winding due to the high frequency currents and magnetic field from the permanent magnet are calculated. The total copper losses are reduced by choosing an appropriate litz wire. To minimize the stator core losses different magnetic materials are compared and it is shown that amorphous and nanocrystalline materials are the best choices. The rotor is designed with a sufficient safety margin for the mechanical stresses. Titanium is used as retaining sleeve material in order to limit the stresses on the high-energy Sm_2Co_{17} magnets.

To verify the analytical calculations a test bench has been built, which consist of two machines (one acting as motor and one as generator) on a common shaft. A common titanium rotor encloses two Sm_2Co_{17} permanent magnets and the stators are constructed using Ni-Fe cores with litz wire in a ring-wound configuration. The critical speeds for the test bench rotor are identified by finite-element analysis. The length of the shaft is adjusted such that rated speed falls between the second and the third bending modes. The measurements on the test bench of the back EMF and the torque match the values obtained by finite-element simulations very well. Further measurements will be carried out with custom-built power and control electronics for motor and generator.

References

[1] S. A. Jacobson and A. H. Epstein, "An informal survey of power mems," ISMME2003, Tsuchiura, Japan, December 1-3, 2003, pp. 513-520.

[2] K. Isomura, S. Tanaka, M. Murayama, H. Yamaguchi, N. Ijichi, T. Genda, N. Saji, O. Shiga, K. Takahashi, and M. Esashi, "Development of micro-turbo charger and micro-combustor as feasibility studies of three-dimensional gas turbine at micro-scale," Proc. ASME Turbo Expo 2003, Power for Land, Sea, and Air, Atlanta, Georgia, USA, June 16-19, 2003, Paper GT2003-38151.

[3] S. Kang, J. P. Johnston, T. Arima, M. Matsunaga, H. Tsuru, and F. B. Prinz, "Micro-scale radial-flow compressor impeller made of silicon nitride - manufacturing and performance," Proc. ASME Turbo Expo 2003, Power for Land, Sea, and Air, Atlanta, Georgia, USA, June 16-19, 2003, Paper GT2003-38933.

[4] J. Peirs, D. Reynaerts, and F. Verplaetsen, "Development of an axial microturbine for a portable gas turbine generator," Journal of Micromechanics and Microengineering, vol. 13, no. 5, 2003, pp. 190-195.

[5] M. K. Senesky and S. R. Sanders, "A millimeter-scale electric generator", IEEE Industry Applications Conference 2004, Conference Record of the 39th IAS Annual Meeting, Seattle, USA, October 3-7, 2004, vol. 1, pp. 346-352.

[6] A. H. Epstein, "Millimeter-scale, mems gas turbine engines," Proc. ASME Turbo Expo 2003, Power for Land, Sea, and Air, Atlanta, Georgia, USA, June 16-19, 2003, Paper GT2003-38866.

[7] P. L. Chapman and P. T. Krein, "Micromotor technology: electric drive designer's perspective," IEEE Industry Applications Conference 2001, Conference Record of the 36th IAS Annual Meeting, Chicago, Illinois, USA, Septemper 30-October 4, 2001, vol. 3, pp. 1978-1983.

[8] U. Kafader and J. Schulze, "Similarity relations in electromagnetic motors - limitations and consequences for the design of small dc motors," ACTUATOR 2004, 9th International Conference on New Actuators, Bremen, Germany, June 14-16, 2004, pp. 309-312.

[9] N. Bianchi, S. Bolognani, and F. Luise, "Potentials and limits of high-speed pm motors," IEEE Trans. Industry Applications, vol. 40, no. 6, pp. 1570-1578, Nov.-Dec. 2004.

[10] J. Peirs, P. Vleugels, T. Waumans, M. Verlinden, D. Reynaerts, and F. Verplaetsen, "Development of high-speed bearings for micro gas turbines," MME'04, 15th MicroMechanics Europe Workshop, Leuven, Belgium, September 5-7, 2004, pp. 313-316.

[11] M. Salehi, H. Heshmat, J. F. Walton II, and M. Tomaszewski, „Operation of a mesoscopic gas turbine simulator at speeds in excess of 700,000 rpm on foil bearings," Proc. ASME Turbo Expo 2004, Power for Land, Sea, and Air, Vienna, Austria, June 14-17, 2004, Paper GT2004-53870.

[12] K. Reichert, "A simplified approach to permanent magnet motor characteristics determination by finite-element methods", 16th International Conference on Electrical Machines ICEM, Cracow, Poland, September 5-8, 2004.

[13] J. A. Ferreira, Electromagnetic modeling of power electronic converters. Norwell, Massachusetts: Kluwer Academic Publishers, 1989, ch. 6.

[14] S. P. Timoshenko and J. N. Goodier, Theroy of elasticity. McGraw-Hill Kogakusha, Ltd. 1970, ch. 4.